Investigation on Flow Characteristics and Parameters Optimization of a New Concept of TC Nozzle

F. Song, L. Zhou†, J. W. Shi and Z. X. Wang

*Shaanxi Key Laboratory of Internal Aerodynamic in Aero-Engine, School of Engine and Energy,
Northwestern Polytechnical University, Xi'an, Shaanxi, 710129, China*

†Corresponding Author Email:*zhouli@nwpu.edu.cn*

ABSTRACT

Lighter weight, simpler structure and throat area controllable are the developing trends of aircraft engine exhaust system. To meet these challenges, a new concept of hybrid throat control (*TC*) nozzle was proposed to improve the control efficiency of throat area (η) by using a rotary valve with secondary injection. The flow mechanism of the hybrid *TC* nozzle and the effect of aerodynamic and geometric parameters on nozzle performance were investigated numerically. Then the approximate model characterizing the hybrid *TC* nozzle was established with design of experiment and response surface methodology. The approximate model was used to analysis the coupling effect between parameters and optimized the parameter combination. The results show that the flow area of the nozzle can be restricted effectively by the rotary valve and the secondary flow, and η is bigger than 5.24. Nozzle pressure ratio and secondary pressure ratio are the dominant factors for the nozzle throat area control performance. The optimization of the parameter combination was carried out with penalty function approach, with ratio of throat area control being 30 percent and corrected mass flow ratio of secondary flow being 5 percent The maximize error of the optimization result is 4.13 percent and it verifies the validity and feasibility of the approximate model.

Keywords: Throat area control; Hybrid *TC* nozzle; Flow characteristics; Approximate model; Performance optimization.

NOMENCLATURE

A_s	area ratio of the throat of the rotary valve to the nozzle throat	P^*	total pressure
A_8	area of nozzle throat	P^*_{pri}	total pressure of the primary flow
A_9	nozzle outlet area	R	radius of valve
C_{fg}	thrust coefficient	R_1	gas constant
CFD	computational fluid dynamics	RSM	respond surface methodology
DOE	design of experiment	RTAC	ratio of throat area control
F_{ac}	actual thrust	SPR	total pressure ratio of the secondary flow to the primary flow
F_{id}	ideal isentropic thrust		
$F_{id, tot}$	the sum of ideal isentropic thrust of primary flow, secondary flow and entrainment flow	SVC	shock vector control
		T^*	total temperature
FTV	fluidic thrust vectoring	T^*_{pri}	total temperature of primary flow
h_{au}	the auxiliary penetration depth supplied by the rotary valve	T^*_{sec}	total temperature of secondary flow
		TC	throat area control
h_{tot}	the penetration depth of secondary flow	v_x	axial velocity
k	specific heat ratio	$W_{ac,pri}$	actual mass flow rate of primary flow
K	a constant determined by gas constant and specific heat ratio	$W_{ac,sec}$	actual mass flow rate of secondary flow
		$W_{id,pri}$	ideal mass flow rate of primary flow
Ma	Mach number	X_L	the half length of experiment plane
NPR	total pressure ratio of the primary flow to the ambient pressure	X^*	the axial length of the nozzle\
p_0	the static pressure of the free stream	η	efficiency of throat area control
p_a	ambient pressure	θ	deflection angle of the rotary valve
P	static pressure	ρ	density
		ω	corrected mass flow ratio of secondary flow

1. INTRODUCTION

Thrust vectoring is one of the critical technologies for next generation of fighter aircraft and launch vehicles. It can improve the agility, maneuverability and control effectiveness of vehicles, as well as the performance of short take-off and landing. However, thrust vectoring conventionally based on complex actuation and control system can bring about complexity and weight punishment what goes against the requirement of high efficiency and light weight for propulsion system (Mason *et al.* 2004). As far as the existing technology, fixed-geometry nozzle is one promising idea. Fluidic injection is injected into the fixed geometry nozzle to make the primary flow deflection and control the vector angle. And the fluidic thrust vectoring (*FTV*) can be achieved with shock vector control (*SVC*) (Heidari and Pouramir, 2016; Younes and Hickey, 2020), dual throat (Ferlauto and Marsilio, 2017), co-flow (Heo and Sung, 2012) and so on. Fixed-geometry can not only reduce the cost and weight, but also the drag and signature (Deere 2003). Therefore, *FTV* technologies, especially SVC, have earned a lot of attention.

However, as for the turbofan engine of fighter aircraft, throat area control (*TC*) is another inescapable issue. In majority conditions, the nozzle operates in a normal mode. But when the maximum thrust is desired, the afterburner is activated, and the nozzle exhaust temperature rises dramatically. Meanwhile, the nozzle throat area is augmented to keep the nozzle flow capacity and the area may be doubled in size. The conventional method used to adjust the throat and outlet to the required size is mechanical control system what undoubtedly adds weight and complexity to exhaust system. Then, the fluidic *TC* was proposed to settle these problems (Martin *et al.* 1957). The effective flow area can be continuously varied over a wide range by suitable injecting a secondary injection into the nozzle throat.

Therefore, if the fluidic *TC* cannot be achieved in the fixed-geometry nozzle, the gain from *FTV* can be compromised, and the practicability of fixed-geometry nozzle is reduced. In contrast to *FTV*, fluidic *TC* has not received enough attention in recent years.

The researches of fluidic *TC* can be traced back to 1950s. An investigation of this method of varying the effective flow area of a convergent nozzle was conducted at NACA Lewis laboratory (Martin 1957). A first-order approximations to the aerodynamic quantities relating to the nozzle was proposed basing on the theory of one-dimensional gas flow without counting the heat exchange between the jet and primary flow. McArdle (1958) used both theoretical analysis and experimental methods to study the effect of design and operating variables (e.g. primary and secondary flow pressure, temperature and injection-slot location) on *TC* of convergent nozzle, and the effective flow area was reduced as much as 67 percent. This method was applied to rocket thrust control by Blaszak and Fahrenholz (1960). They concluded that significant flow throttling could be achieved through secondary injection, and throttling effect was sensitive to the injection angle but insensitive to primary pressure ratio or orifice arrangement (slot versus holes, etc.) in symmetric and asymmetric injection. Additionally, a relatively simple analytical flow model was devised. Zumwalk and Jackomis (1962) discovered that the effect of the throat area would be weakened if the direction of the injection was same as that of the primary flow.

In the 1970s and 80s, researchers were attracted by the mechanical vectoring nozzles and the research on throat area control was interrupted once. In 1990s, LMTAS, P&W and USAF WL took part in the Fluidic Injection Nozzle Technology program sponsored by the US Air Force and NASA to investigate the fluidic *TC* technology, especially how to get satisfactory ratio of throat area control (*RTAC*) with limited secondary flow(Walker 1997). Catt *et al.* (1995) and Miller and Catt (1995) utilized a cost-effective computational fluid dynamics (*CFD*)/Design of experiment (*DOE*) methodology to identify key parameters for enhanced injection effectiveness. The effects of geometry of the nozzle and injection properties on discharge coefficient, thrust coefficient (C_{fg}) and *RTAC* were investigated, and the final *RTAC* reached 49 percent with the secondary flow rate being 15 percent of the primary flow. Moreover, they studied the effect of secondary pressure ratio and injection schemes with *CFD* and experimental methods. LMTAS conducted a series of researches on fluidic *TC* with pulse injection (Vakili *et al.* 1999; Miller *et al.* 2001; Domel *et al.* 2007; Baruzzini *et al.* 2007). The results indicated that pulse injection was not superior to steady injection.

The working principle and the effect of parameters of fluidic *TC* are preliminarily revealed. But there are still several unsolved issues. One is the low efficiency of the throat area control (η). In order to ensure that the engine can work stably under extreme conditions, such as afterburning condition, the fluidic *TC* needs to be activated under normal unaugmented mode and the corresponding *RTAC* may reach a larger value. On the current technical level, it means that a great deal secondary injection from fan or compressor is almost necessary when the afterburner is not activated which causes severe degradation of aero-engine performance.

In order to improve η, a concept of hybrid *TC* nozzle consisting of a basic two-dimensional convergent-divergent nozzle and a rotary valve in the throat was proposed in this paper. The idea is developed from the application of simple mechanical device in SVC (Shi *et al.* 2020; Thillaikumar *et al.* 2020). The simple mechanical device is used to enhance or replace the effect of fluid injection without significant increase in weight and complexity for nozzle. The original intention of the hybrid *TC* nozzle is to improve η with simple mechanical auxiliary device and to achieve the target *RTAC* with as little secondary flow as

possible. The flow mechanism of the hybrid *TC* nozzle and the effect of aerodynamic and geometric parameters are studied numerically in the following parts of this paper. The performance estimation model for hybrid *TC* nozzle is established based on *DOE* and Respond Surface Methodology (*RSM*). With the approximate model, the coupling effect of the aerodynamic and geometric parameters is studied and the optimization of parameter combination is performed.

2. THE WORKING PRINCIPLE AND NUMERICAL APPROACH

2.1 Working Principle of a Hybrid *TC* Nozzle

The injection slots of fluidic *TC* nozzle are replaced by rotary valves, as shown in Fig. 1. The valve can be rotated around the axis and the state of the valve can be transformed from open to close, or vice versa. When hybrid *TC* nozzle works, the symmetrically distributed values are opened simultaneously and a secondary injection extracted from the high pressure components, fan or compressor, is then injected into the near-sonic primary flow. A certain penetration depth of the secondary flow is formed and the primary flow is blocked effectively. As a result, the effective throat area is smaller than the nozzle throat area (A_8), as shown in Fig. 2. Compared with the fluidic *TC* nozzle, the rotary valves could supply an auxiliary penetration depth for the secondary flow which can enhance the blocking effect of the fluidic injection. Moreover, the rotary valves can be used to control *RTAC* through changing the deflection angle. Additionally, the symmetrically entrainment tunnel is employed in the hybrid *TC* nozzle to reduce the flow loss under over-expansion condition. The entrainment tunnel is set open in this study with constant total pressure which is slightly higher than ambient pressure.
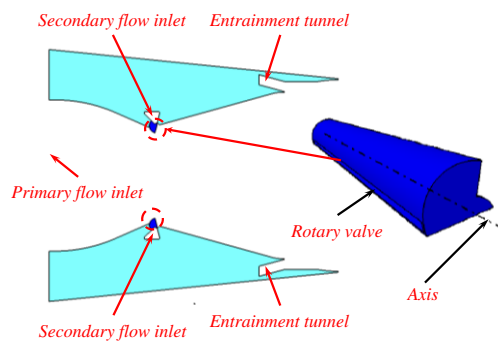

Fig. 1. Structure of the hybrid *TC* nozzle.

2.2 Simulation Scheme and Turbulent Model

The numerical simulation in this paper was performed with Fluent 14.0. The being considered compressible Reynolds-averaged Navier-Stocks equations in this work are discretized in the finite-

volume form for each hexahedral control volumes. Second-order upwind scheme is employed in the spatial discretization, and second implicit scheme is adopted for time. The implicit density-based algorithm is selected to solve the equation, and Foe-FDS is chosen for the flux type. In the solving course, the varying specific heat and the effects of temperature on viscosity coefficient are taken into account.
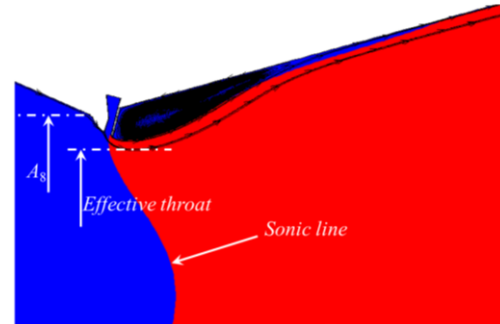

Fig. 2. Demonstration of throat area control effect.

The flow features of the hybrid *TC* nozzle are dominated by disturbance in the subsonic primary flow with the transverse injection of secondary flow and the rotary valve. During the simulation, the turbulence model directly affects the resultant flow details. As is studied, the results under different turbulence models appear diversely under varying *SPR*s. Therefore, in this work, the validation of the turbulence model was performed beforehand. It was validated by comparing the simulation results with the experimental data obtained by Spaid and Zukoski (1968). In their work, a plane with an injection slot is placed in the wind tunnel and the direction of the injection slot is perpendicular to the velocity direction of the free stream. The free stream Mach number (*Ma*) is 2.61 and the ratio of injection total pressure to free stream total pressure is about 1.15.

Several turbulence models, including Spalart-Allmaras (*SA*) model, Shear Stress Transport (*SST*) *k-ω* model, and Renormalization Group (*RNG*) *k-ε* model, were chosen to perform the simulation work and the static pressure distribution at the centerline for the plane and flow field predicted by *SST k-ω* are shown in Fig. 3. The *X* coordinate is nondimensionalized by the half length of experiment plane (X_L) and the *Y* coordinates in Fig. 3(a) and (b) are nodimensionalized by free stream static pressure (p_0) and X_L respectively. It can be seen that, *SST k-ω* turbulence model with compressible-flow effect exhibits high capability in predicting the distribution of the pressure on upstream and downstream walls of the injection slot. The result predicted by the model can match the experiment result more closely when the distance between the first layer of grid and the wall is 1×10^{-6} m and the corresponding y^+ is about 1.0. Thus, *SST k-ω* turbulence model with compressible-flow effect was selected to study the flow characteristics of the hybrid *TC* nozzle.
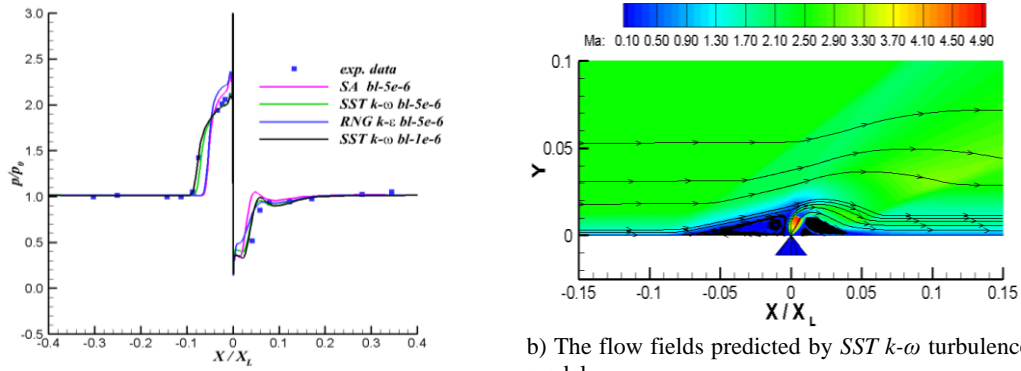
a) The comparison of static pressure at centerline between the predicted results and experiment data

b) The flow fields predicted by *SST k-ω* turbulence model

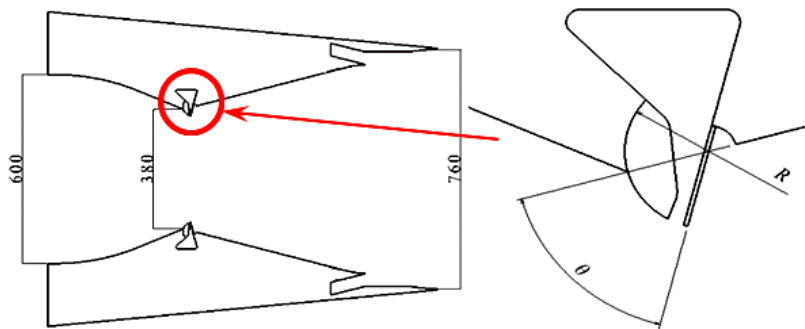**Fig. 3. Comparison of pressure distribution between experiment data and obtained from different turbulent model.**

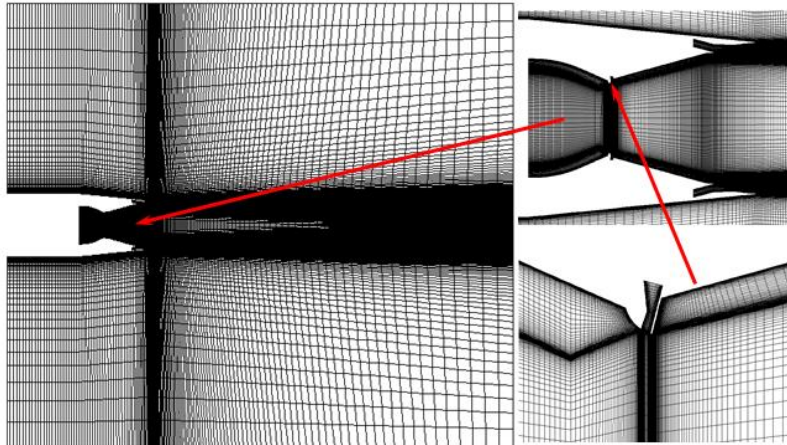**Fig. 4. Geometric model of the hybrid *TC* nozzle.**

Fig. 5. Computational grid.

2.3 Geometric Model and Computational Grid

The details of geometric parameters and the configuration of a hybrid *TC* nozzle are shown in Fig. 4. The expansion ratio (the area ratio of nozzle outlet area to the throat area, A_9/A_8) of the hybrid *TC* nozzle is 2. For the design condition, the primary flow is supposed to continue to accelerate in the convergent-divergent nozzle without shock waves, and the outlet Ma is high than 1 and the outlet static pressure is equal to ambient pressure. The corresponding total pressure ratio of the primary flow to the ambient pressure (*NPR*)

obtained from the isentropic expansion process is 10. The rotary valves with a convergent-divergent channel are located at the throat of the nozzle. The deflection angle of the valve (θ) is defined as the angle between the rotary valve and the divergent wall of the nozzle. Restricted by the geometry, the maximum value of θ is 60.0°. A_s is defined as the throat area ratio of the valve channel to the nozzle.

The computational grid used in this paper is shown in Fig. 5. The mesh around the rotary valve and near internal walls is refined to predict the details of the flow structure. The valve of y^+ for first layer of grid above the wall is about 1.0. The grid-

dependence analysis was performed before the study of aerodynamic and geometric parameters. Three sets of mesh with the same value of y^+ are selected with 75,000 cells, 145,000 cells and 265,000 cells, respectively. The results shown in Fig. 6 indicate that the deviation in the static wall pressure is not significant among the three grid settings. Parameter X^* represents the axial length of the nozzle. P^*_{pri} is the total pressure of the primary flow. The grid setting with intermediate number of cells was employed for this study.
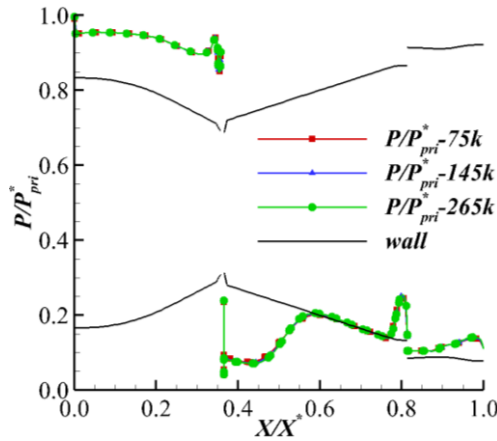
**Fig. 6. Comparison of the results with different mesh densities.**

The difference between two-dimensional and three-dimensional simulation was investigated to ensure that the two-dimensional simulation was feasible. The comparison is shown in Fig. 7. It can be seen that the wall static pressure distributions at symmetry plane obtained from two-dimensional and three-dimensional simulations under various conditions are the same. *RTAC* and ω obtained from the two models are exactly the same and the maximum difference in C_{fg} between the two models is less than 0.75 present. Given the computational efficiency, two-dimensional simulation model was used to capture the key flow characteristics of the hybrid *TC* nozzle in this study.

## 2.4 Boundary Conditions and Parameters Definitions

Pressure inlet boundary condition was specified for the nozzle inlet, the secondary injection inlet, the entrainment flow inlet and the outer flow field inlet. The total pressure, total temperature and flow angle were respectively prescribed for these parts. The nozzle pressure ratio varies from 3 to 14 while the secondary pressure ratio is selected as 0.6, 0.8, 1.0, 1.2, 1.4 and 1.5, increasingly. The effect of inlet total temperature is not considered in this paper.

At the outflow boundary the ambient pressure (p_a) is imposed and the other variables are extrapolated from the interior. The static pressure, the free-stream *Ma* (0.05) and the flow direction are given at the pressure-far-field boundary. Interior boundaries including the nozzle outlet and the secondary

injection outlet are monitored. Impermeable, no-slip and adiabatic boundary condition is applied to the solid wall to ensure zero values for normal flux of mass, momentum and energy across the surface mesh of the wall.
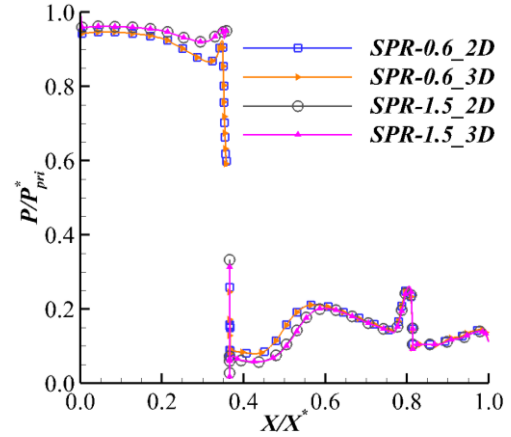
(a) Wall static pressure at symmetry plane
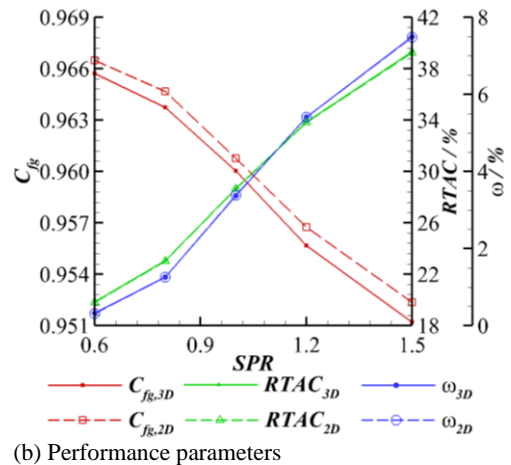
(b) Performance parameters

Fig. 7. Comparison of simulation result obtain from 3D and 2D simulation.

In this paper, three parameters, C_{fg}, *RTAC* and η, are calculated based on the simulation result to assess the performance of the hybrid *TC* nozzle. C_{fg} is the ratio of actual thrust (F_{ac}) to total ideal isentropic thrust ($F_{id,tot}$). F_{ac} is calculated by Eq. (1) and the integration is implemented at nozzle outlet.

$$F_{ac} = \int_{A_9} (\rho v_x v_x + (P - p_a))dA \tag{1}$$

Where ρ, v_x and p represent the density, axial velocity and static pressure at nozzle outlet. $F_{id,tot}$ is the sum of the ideal thrust of primary flow, secondary flow and entrainment flow. The ideal isentropic thrust (F_{id}) of the three flows is calculated with the method illustrated by Eq. (2).

$$F_{id} = W_{ac}\sqrt{\frac{2kR_l}{k-1}}\sqrt{T^*[1-(\frac{p_a}{P^*})^{\frac{\kappa-1}{\kappa}}]} \tag{2}$$
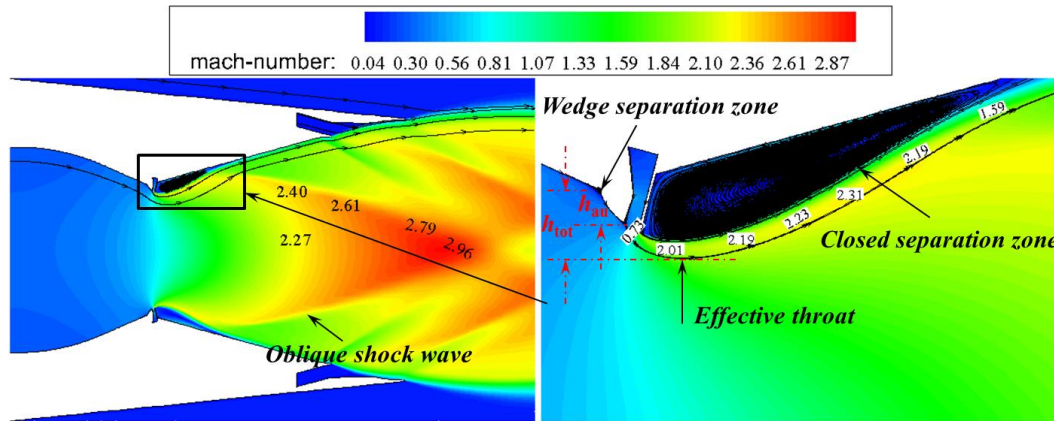
Fig. 8. Typical flow field of a Hybrid *TC* nozzle.

Where W_{ac} is the mass flow rate of primary flow, secondary flow or entrainment flow obtained from simulation. T^* and P^* are the total temperature and total pressure of these airflows. Parameters k and R_1 represent specific heat ratio and gas constant, respectively.

RTAC is defined as

$$RTAC = (W_{id,pri} - W_{ac,pri})/W_{ac,pri} \times 100\% \qquad (3)$$

Where $W_{ac,pri}$ is the actual mass flow rate of primary flow and $W_{id,\,pri}$ is the ideal mass flow at the nozzle throat when the rotary valve is closed. $W_{id,\,pri}$ is solved from Eq. (4).

$$W_{id,pri} = K \frac{P^*_{pri}}{\sqrt{T^*_{pri}}} A_8 \qquad (4)$$

$$K = \sqrt{\frac{k}{R_1}(\frac{2}{k+1})^{\frac{k+1}{k-1}}} \qquad (5)$$

Where K is a constant determined by gas constant and specific heat ratio, and A_8 is the nozzle throat area when the rotary valve is closed and T^*_{pri} is total temperature of the primary flow.

Parameter η is the ratio of *RTAC* to the corrected flow ratio of secondary flow (ω), which is calculated by Eq. (6).

$$\omega = (W_{ac,sec}\sqrt{T^*_{sec}})/(W_{ac,pri}\sqrt{T^*_{pri}}) \times 100\% \qquad (6)$$

Where $W_{ac,\,sec}$ and T^*_{sec} represent the actual mass flow rate and total temperature of secondary flow, respectively.

3. RESULT AND DISCUSSION

3.1 Flow Characteristics of a Hybrid SVC Nozzle

The essential flow characteristics of a hybrid *TC* nozzle lies in the fact that the subsonic flow is transversely injected into the high subsonic primary flow. The secondary flow is extracted from a fan or compressor of an aero-engine. The original purpose of the convergent-divergent channel in the rotary valve is to keep the secondary flow accelerating continuously and being supersonic while encountering the primary flow. And then the energy

of the secondary flow can be translated to momentum in the primary flow normal direction to maximum the penetration depth of the secondary flow. The Ma distribution in nozzle and around the valve is shown in Fig.8. The results indicate that the secondary flow is subsonic when it encounters the primary flow. The expansion of the secondary flow in the convergent-divergent channel is restricted by the primary flow. The subsonic secondary flow is deflected gradually to the direction of the primary flow after it encounters the primary flow. And, the secondary flow continues to expand for the low back pressure in the downstream from the rotary valve and then is restricted by both the internal wall of the nozzle and the primary flow, as shown in Fig. 8. Therefore, the secondary flow undergoes an acceleration followed by a deceleration and be attached to the wall again. Thus, the throat of the convergent-divergent channel is not effective and the effective aerodynamic throat of the secondary flow where Ma reaches 1 locates downstream from the outlet of the channel.

In most cases, there is a bubbly closed separation zone in the downstream from the rotary valve accompanying with an oblique shock at the end of the closed separation zone. A certain penetration depth (h_{tot}) is formed with an auxiliary penetration depth (h_{au}) supplied by the rotary valve.

As for the primary flow blocked by the rotary valve, a wedge separation zone upstream from the rotary valve is formed, as shown in Fig. 8, causing a rise in static pressure (Fig. 9). But given the geometric characteristic of the cylindrical surface of the rotary valve, the wedge separation zone is not as significant as the bubbly closed separation zone downstream. The primary flow then accelerates along the valve's surface before it encounters the secondary flow. Blocked by the secondary flow, the effective flow area of the primary flow is reduced and the effective throat is pushed downstream. The primary flow reaches sonic speed around the effective throat and accelerates further until meeting the internal walls and forming the oblique shock at the end of the closed separation zone. After that, the primary flow is first compressed and then it expands around the outlet of the entrainment

channel, followed by a similar process downstream until the primary flow gets out of the nozzle. The series of changes are caused by the changes in geometry of internal wall around the entrainment channel. The corresponding distribution of the wall static pressure can be seen in Fig. 9. The symmetrical oblique shocks and expansion wave intersects downstream and influence the core flow.

When the nozzle works in severe over-expansion state (*NPR*=3), the primary flow does not have the ability to attach the secondary flow to the internal walls again. Then an open separation zone downstream from the rotary valve is formed and the air from the entrainment channel is induced in the separation zone. The open separation zone and the secondary flow can control the flow area of the primary flow effectively and minimize the flow loss caused by overexpansion.

The secondary flow can form a certain penetrate depth in the primary flow and control the effective throat of the primary flow. Apparently, the valve functions in two ways: firstly, the valve can offer an auxiliary penetration depth to the secondary flow, thus enlarging the *RTAC*; secondly, the valve can change the injecting direction of the secondary flow, thereby adjusting *RTAC* within a certain range.
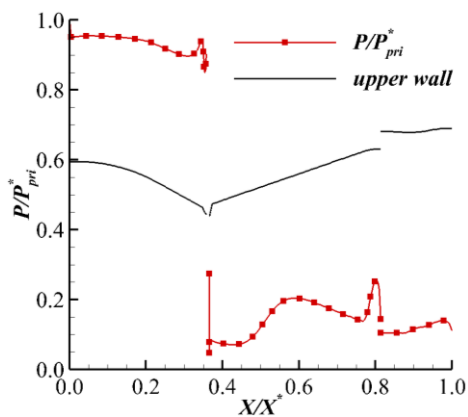

Fig. 9. Distribution of wall static pressure on the symmetry plane.

3.2 The Effect of Key Parameters

A. The Effect of *NPR*

With increasing *NPR* from 3 to 14, the working state of the nozzle is expected to change from overexpansion to underexpansion condition and the interaction between the primary flow and the secondary flow is changed.

In the convergent-divergent nozzle, the static pressure of the primary flow drops accompanied by acceleration from subsonic speed to supersonic speed. In the severe over-expansion state (*NPR*=3), the primary flow lacks potentiality to expand and accelerate in the divergent section. The static pressure of the primary flow is too low to attach the secondary flow to internal walls. An open separation zone is formed downstream from the

rotary valve, and the air from the entrainment channel is induced in it. As a result, the penetration depth of the secondary flow is deeper, as shown in Fig. 10. Meanwhile, the open separation zone leads to the increase in the mass flow rate and the speed of entrainment air. The static pressure of the entrainment air drops as the total pressure does not change. Finally, the static press around the outlet of entrainment channel is lower than the ambient pressure which causes reverse flow of the external flow around the nozzle outlet, as shown in Fig. 10. The flow area of the primary flow is restricted by the secondary flow, the open separation zone, the entrainment air and the reverse flow, as well as the expansion of the primary flow and the flow loss caused by overexpansion. But a normal shock near the nozzle outlet is still essential for primary flow to match the ambient pressure.

When *NPR* is higher than 4, the secondary flow is attached to the internal walls and a closed separation zone is formed. Considering that all the calculation points satisfy the geometric similarity and enter the self-modeling region, it could be concluded according to the similar theory that the flow characteristics around the throat of the nozzle are similar for the same *Ma* distribution, as shown in Fig. 11. Therefore, *RTAC, ω* and *η* remain approximately unchanged with increasing *NPR* from 4 to 14, as shown in Fig. 12. And the minimum *η* is 8.46. But the variety of C_{fg} is obvious. When the *NPR* is 4, the primary flow suffers a severe expansion process in the divergent section of the nozzle and a strong normal shock is formed near the nozzle outlet causing a severe flow loss, even though the primary flow is still restricted by the open separation zones (Fig. 10). With the further increase of *NPR*, the working state of the nozzle changes to optimum-expansion and the corresponding C_{fg} increases (Fig. 12). But when the throat area control is activated, the effective expansion ratio of the hybrid *TC* nozzle is bigger than 2. The corresponding optimal *NPR* exceeds 10, or even 14. The result indicates that the optimum *NPR* for the nozzle is no less than 14.

B. The Effect of *SPR*

The backpressure around the outlet of the valve's channel is constant, because the subsonic primary flow undergoes the same expansion process in the convergent section before it encounters the secondary flow. Therefore, the flow capacity of the valve's channel is enhanced and the momentum per unit mass of the secondary flow increases with the increase of *SPR*, as well as the penetration depth of the secondary flow (Fig. 13). When *SPR* is 0.6, the ratio of the inlet total pressure and outlet static pressure for the valve's channel is too low and the corresponding *ω* is only 0.3 percent which means an extremely poor flow capacity for the valve's channel. But the *RTAC* is still 20 percent because of the existence of the rotary valve, and *η* is surprisingly high. With the increase of *SPR*, the auxiliary penetration depth of the rotary valve keeps unchanged. Then the increase of *RTAC* is more slowly than *ω*, and *η* reduces with the increase of *SPR* (Fig .14). The minimum *η* is 5.24.
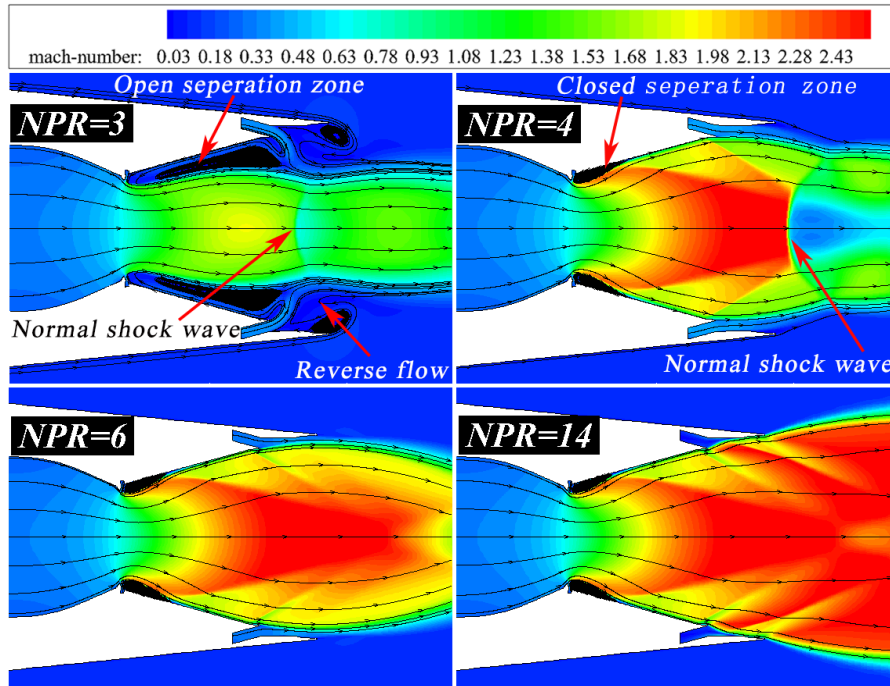
Fig. 10. Effect of *NPR* on the *Ma* distribution.
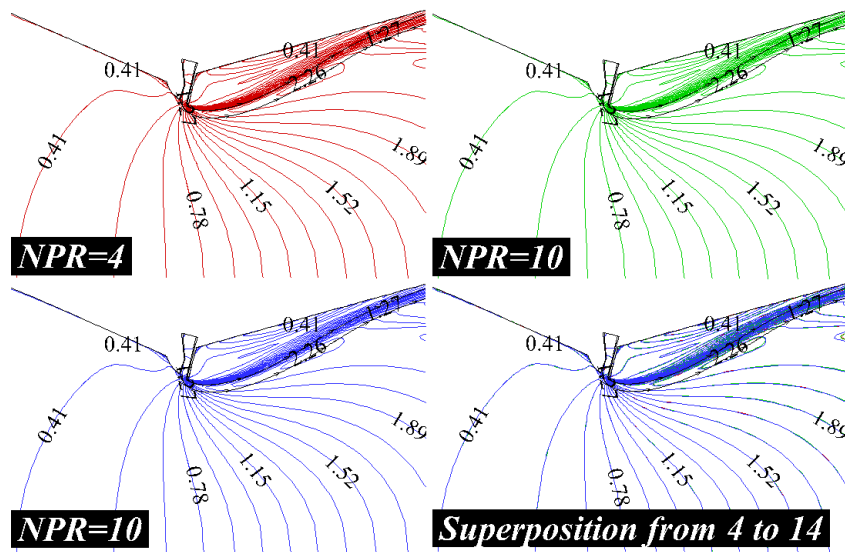

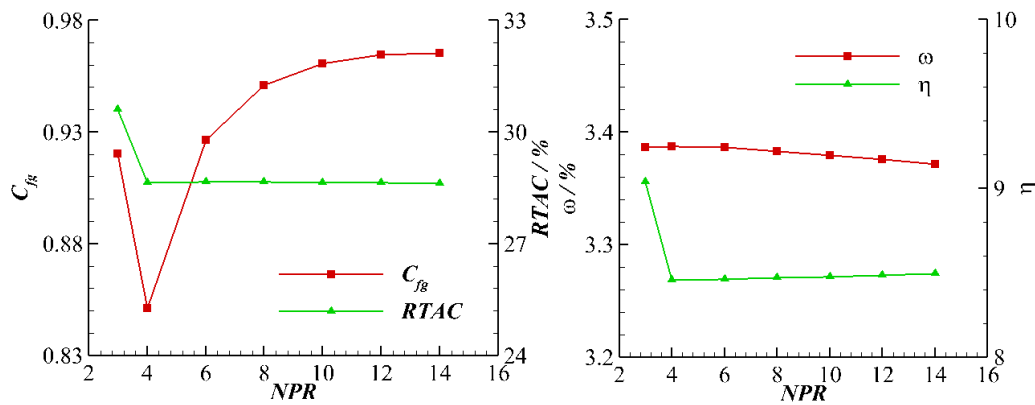**Fig. 11. Distribution of *Ma* near the throat.**

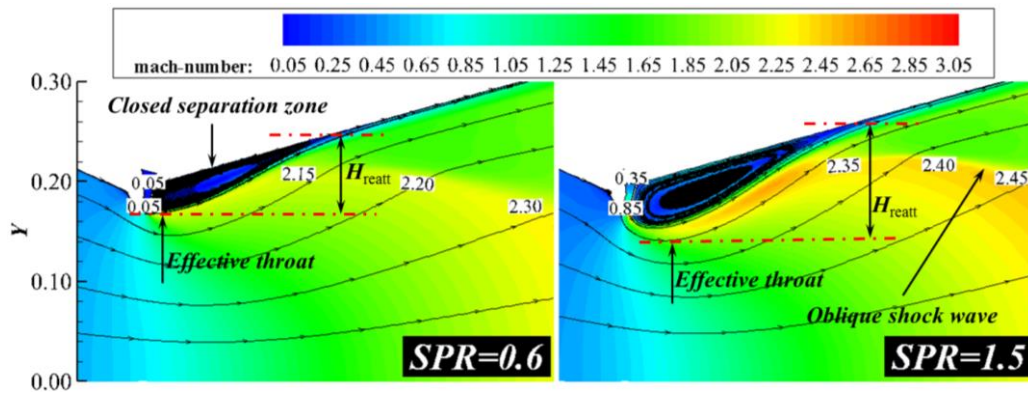**Fig. 12. Effect of *NPR* on the nozzle performance.**

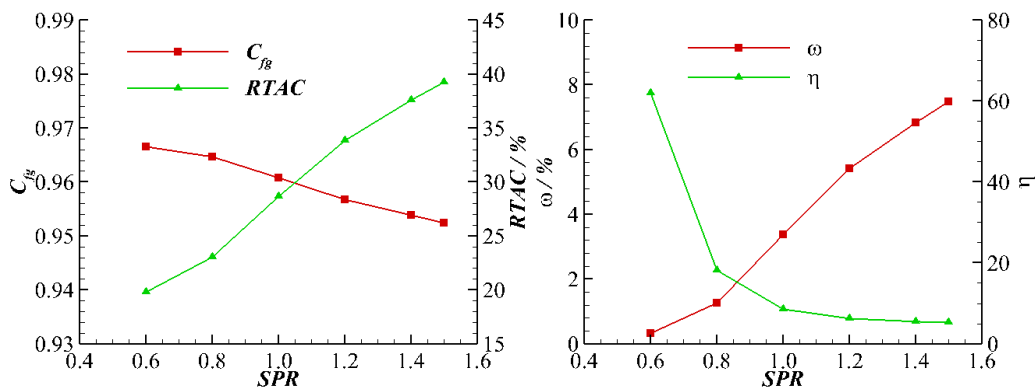**Fig. 13. Effect of *SPR* on the *Ma* distribution.**

Fig. 14. Effect of *SPR* on nozzle performance.

There are two factors what results in the reduction of the C_{fg}. Firstly, with the increase of the *SPR*, the effective throat decreases and the location where the secondary flow is attached to the internal walls moves downstream. As a result, the distance between the effective throat and end point of the closed separation zone, H_{reatt}, increases. It means the primary flow goes through a more severe expansion process and the oblique shock at the end of the separation zone would intensify which leads to severer flow loss. Secondly, with the increasing of the *SPR*, the effective throat area decreases but the nozzle outlet area is constant. Then the effective expansion ratio of the nozzle increases, and the nozzle suffers severer overexpansion leading to a further increase in flow loss.

C. The Effect of θ

The rotary valve can be employed to supply an auxiliary penetration depth for the secondary injection and to control the injecting direction of the secondary flow. The increase of θ has a significant influence on the flow characteristics.

Firstly, the outlet of the valve's channel moves downstream and the injecting direction of the secondary flow would deflect to the normal direction of the primary flow with the increase of θ, as shown in Fig. 15. Therefore, the primary flow undergoes a longer acceleration process before encountering the secondary flow and the momentum of the secondary flow in the reverse

direction of primary reduces causing a decrease in the static pressure around the outlet of the valve's channel. As a result, the mass flow rate of the secondary flow increases, as well as the total momentum. Secondly, the auxiliary penetration depth supplied by the rotary valve increases with the increase of θ. Thirdly, the secondary flow deflects to the normal direction of the primary flow. It means that the normal momentum of the secondary flow increases. However, determined by the geometric characteristic of the rotary valve, the increase in auxiliary penetration depth and normal momentum is noticeable when θ is smaller than 45.0°. Therefore, the penetration depth of the secondary flow cannot increase as fast as ω, and η first increases and then decreases along with the increase of θ, as shown in Fig. 16. And the minimum η is 8.20. Meanwhile, because of the stronger oblique shock wave and the severer overexpansion caused by the increase in θ, the flow loss increases leading to the decrease of C_{fg}.

D. The Effect of *R*

The increase of *R* from 20 to 40 mm functions in two ways. Firstly, the auxiliary penetration depth increases and the increase of the auxiliary penetration depth contributes to the increase of *RTAC*. Secondly, the primary flow undergoes a longer acceleration process before encountering the secondary flow causing a decrease in the static pressure around the outlet of the valve's channel (Fig.17). The discharge coefficient of the secondary
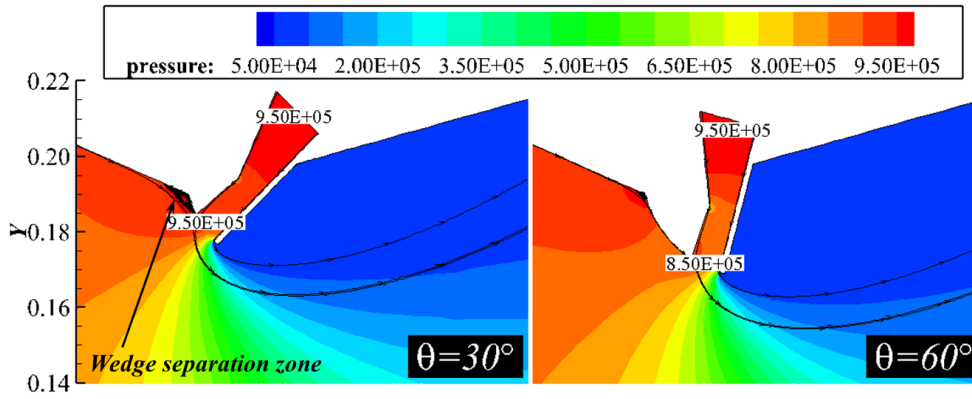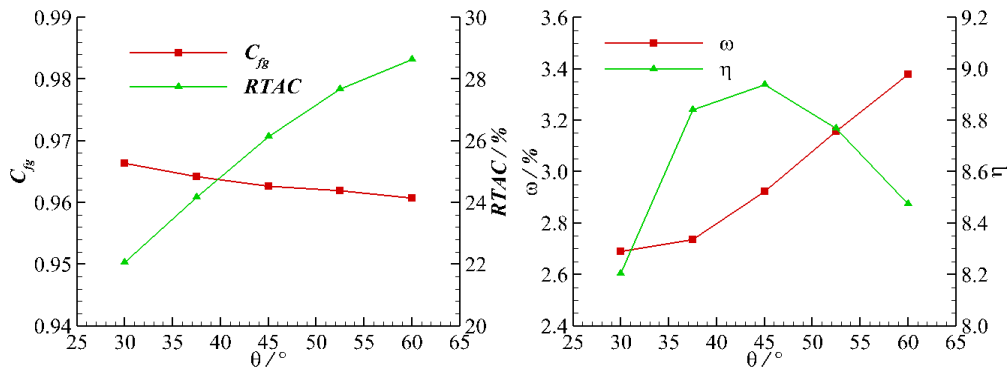
Fig. 15. Effect of θ on static pressure distribution.

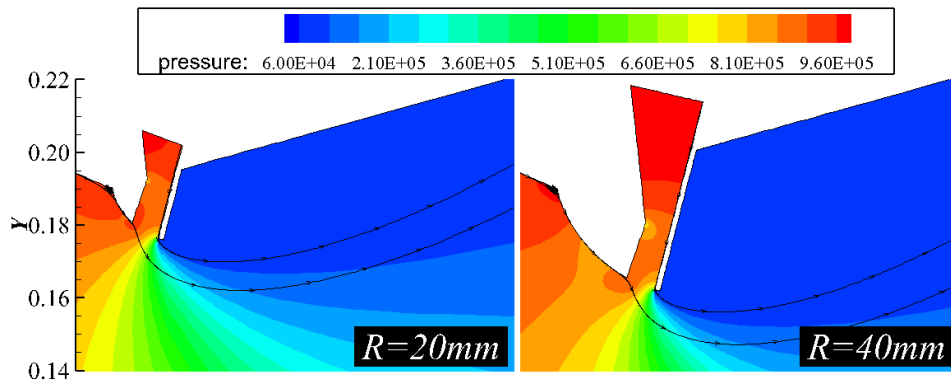**Fig. 16. Effect of θ on nozzle performance.**

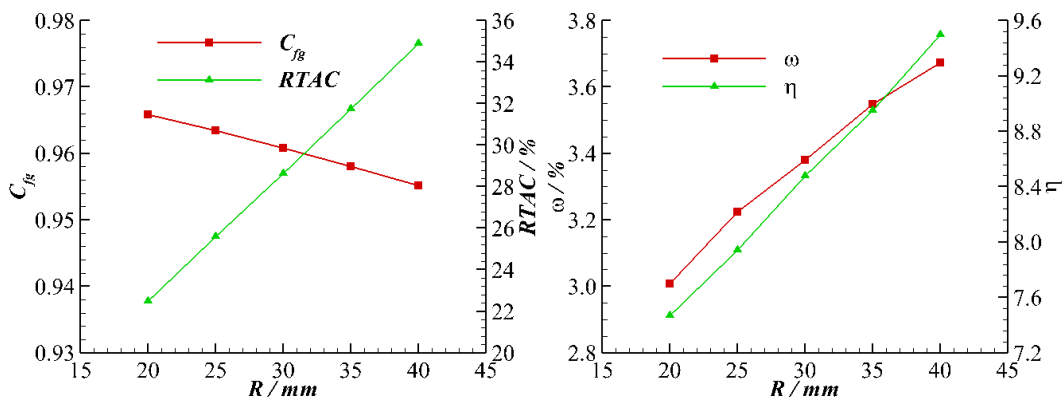**Fig. 17. Effect of R on static pressure distribution.**

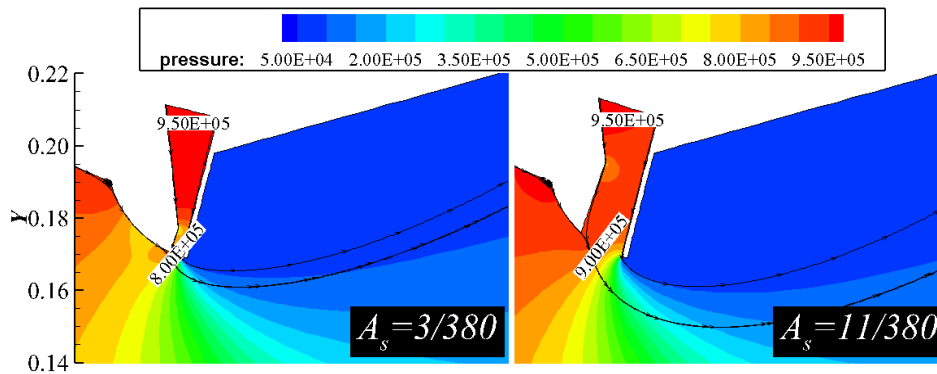**Fig. 18. Effect of R on nozzle performance.**

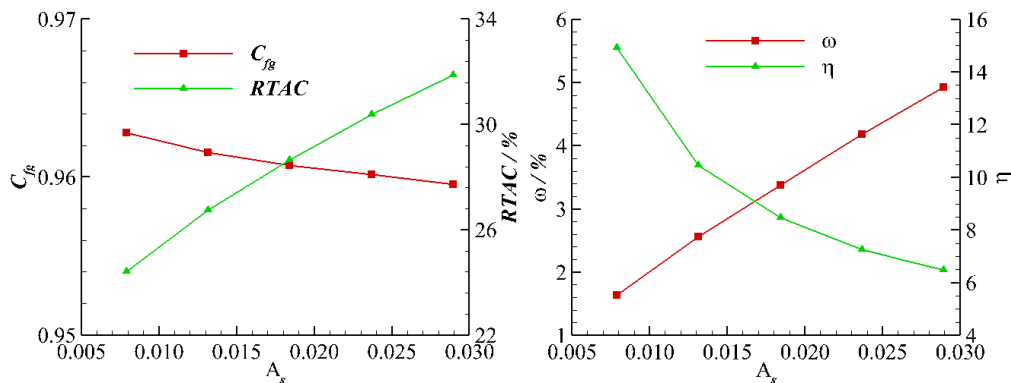**Fig. 19. Effect of A_s on static pressure distribution.**

Fig. 20. Effect of A_s on nozzle performance.

flow increases from 0.667 to 0.739 and it means the increase of mass flow rate for the secondary flow. What's more, the secondary flow can reach deeper depth in the primary flow which is beneficial to the increase of η. Therefore, *RTAC* and η increase with the increase of R, as shown in Fig. 18. And the minimum η is 7.46.

E. The Effect of A_s

Keeping the same expansion ration for the valve's convergent-divergent channel, the change in the geometry of the rotary valve caused by the increase of A_s from 3/380 to 11/380 can be seen in Fig. 19. With the increase of A_s, the lead edge of the valve's channel outlet moves upstream. It leads to a shorter expression process of primary flow before encountering the secondary flow. It means that the backpressure of the valve's channel increases and the flow capacity of the channel is restricted. The corresponding discharge coefficient decreases from 0.832 to 0.645, even though the mass flow rate of secondary increases. The total momentum of the secondary flow increases with the increase of the mass flow rate. As a result, *RTAC* increases. Given that the auxiliary penetration depth contributed by the valve is constant, η decreases with the increase of A_s, as shown in Fig. 20. And the minimum η is 6.47.

3.3 Optimization of the Critical Parameters

The flow mechanism of the hybrid *TC* nozzle and

the effect of aerodynamic and geometric parameters are revealed in previous sections. However, all the previous work tends to bias results to one region of the design space and may not produce satisfactory results over a wide range of experimental settings. In order to assess the performance of complex systems involving multiple parameters, a full-factorial set of experiments can be conducted to set all possible combinations of variables and it is the most accurate method when trying to characterize a complex system. This provides a complete map of design space and can estimate interactions among factors. However, this approach is very labor-intensive. In this paper, five parameters are involved and three or more levels of each parameter are estimated to assess the non-linear variations. A full-factorial would require 3^5 or even more experiments.

DOE can provide a statistically significant subset of a full factorial. Compared to single permutation design, it provides a more balanced representation of the design space. And it is more mathematically robust since it relies on all experiments to define the effect of each independent factor. Box-Behnken Design (*BBD*) is one of the most commonly used *DOE* methods. It is characterized by establishing polynomial consisting of linear terms and quadratic terms with as few experiment points as possible. The all experiment points of *BBD* are equidistant from the design point.

And then *RSM* is used to establish the approximate

model of the complex system in this work. The response functions (P_j) on design factors (X_i), as shown in Eq. (7), are obtained with polynomial regression. The polynomial coefficients (β) are solved with standard least-square method and the result is verified with variance (R^2).

$$P_j = \beta_0^j + \sum_{i=0}^{n} \beta_i^j X_i + \sum_{i=0}^{n} \beta_{ii}^j X_i^2 + \sum_{i \neq k}^{n} \beta_{ik}^j X_i X_k \qquad (7)$$

A. The Establishment of *RSM* Model Based on *DOE*

Based on the previous research, all the five parameters can affect the nozzle performance significantly. Therefore, these five parameter including three geometric parameters and two aerodynamic factors are selected as control factors to characterize the hybrid *TC* nozzle. And three performance parameters, *RTAC*, C_{fg} and ω are used as response values. The range of each control factor is shown in Table 1. All the response values changes discontinuously when *NPR* increases from 3 to 4. The discontinuous change cannot be captured exactly by the quadratic polynomial. Therefore, *NPR* ranges from 4 to 14. The range of other factors is the same as that of previous work.

The experiment design based on *BBD* with five control factors includes 41 points. All the 41 points were simulated with same method introduced in Section 2. Then all the corresponding three response values were extracted from computational results to establish the approximate model.

Finally, the regression of quadratic polynomial coefficient was solved. The significance analysis was done and step regress was used to filter unimportant factors, and to obtain the polynomial coefficients. The final results of variance analysis are listed in Table 2. It can be seen that all three variances are greater than 0.99 and the approximate model can satisfy precision demand perfectly. The approximate model can be used to characteristic the hybrid *TC* nozzle theoretically.

Table 1 Design space of *DOE*

	NPR	*SPR*	A_s	*R/mm*	$\theta/°$
Lower	4	0.6	3/380	20	30
Upper	14	1.5	11/380	40	60

Table 2 Result of variance analysis

	RTAC	C_{fg}	ω
R^2	0.999	0.995	0.997

With the *RSM* model, the Pareto graphs for all the three response value were plotted to illustrate the contribution rate of all linear and quadratic terms (Fig. 21 to Fig. 23). Only the top five terms are shown here and the blue and red color are used to represent positive effect and negative effect respectively. *SPR*, *R* and A_s are the main influence on *RTAC*. The effect of *NPR* on *RTAC* is negligible and the result is same as the result obtained from

previous research. *NPR* is the dominant factor for C_{fg} and the three geometric parameters have no remarkable effect on C_{fg}. As for ω, *SPR* and A_s are the main influence. It is valuable for the hybrid *TC* nozzle that θ can influence *RTAC* significantly without decreasing C_{fg} apparently. It means that θ has the potential to be used to regulate *RTAC* in various working conditions.

For a complex system involving multiple parameters, there are complex coupling effects between parameters. In Fig. 21 and Fig. 23, it can be seen that the effect of the quadratic term, A_s*SPR, on the nozzle performance is significant. Another feature of the *RSM* model is that the coupling effect or interaction between factors can be studied easily. *RTAC* increases along with the increase of A_s when *SPR* is 1.5 but the trend is opposite when *SPR* is 0.6, as shown in Fig. 24. The similar coupling effect on ω is shown in Fig. 25.
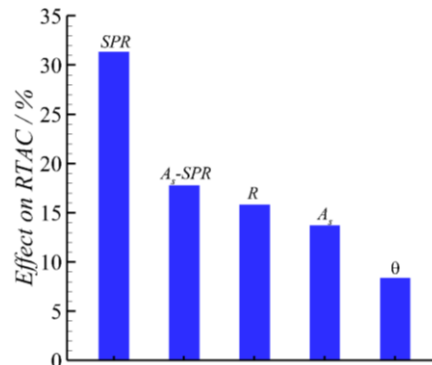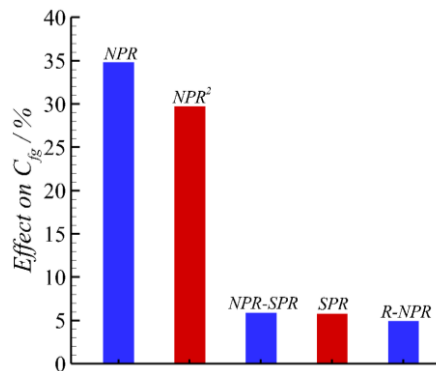

Fig. 21. Pareto graph of *RTAC*.

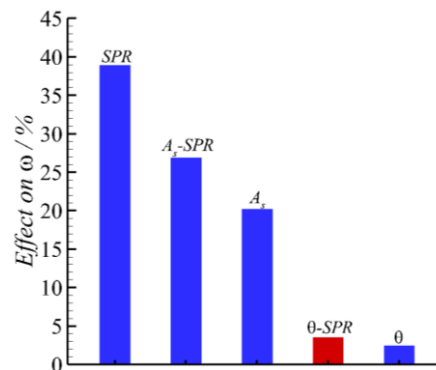**Fig. 22. Pareto graph of C_{fg}.**

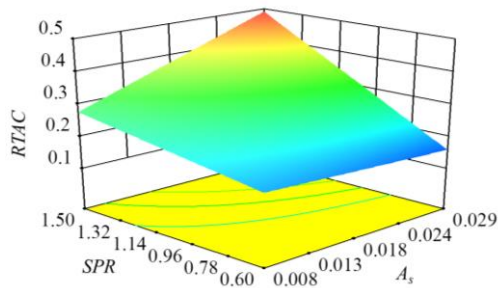**Fig. 23. Pareto graph of ω.**

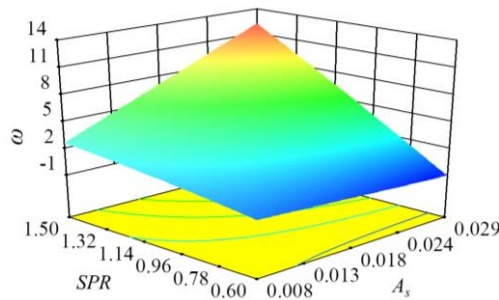**Fig. 24. Interaction effect of critical parameters on *RTAC*.**

Fig. 25. Interaction effect of critical parameters on *ω*.

B. Optimization and Validation

Penalty function approach was used to optimize the combination of aerodynamic and geometric parameters after getting the quadratic polynomial. This would be useful to find one or some parameter combinations in the design space to satisfy design requirements. In this paper, one case is done and validated by CFD. The aim in this case is to make the *RTAC* reach 30 percent with *ω* being 5 percent. The optimization result is showed in Table 3. Then the optimization result is validated with CFD and the result is shown in Table 4. It can be seen that the maximize error is 4.13 percent which is still smaller than 5 percent and the prediction results for *RTAC* and C_{fg} agree with the CFD results.

Table 3 Optimization result

NPR	*SPR*	*θ*	A_s	*R*	C_{fg}
6.96	1.26	42.24	0.0171	27.54	0.926

Table 4 Validation of optimization result

	RTAC/%	C_{fg}	*ω*
RSM	30.0	0.926	5.000
CFD	30.6	0.939	5.216
Error/%	-2.09	-1.39	4.13

4. CONCLUSION

In this paper, a new nozzle structure, namely the hybrid *TC* nozzle, was proposed and it could be used to improve the efficiency of fluidic *TC* with a simpler mechanical auxiliary device, and to reach the desired *RTAC* with as little secondary flow as possible. A computational study was conducted to investigate the flow mechanism of the hybrid *TC* nozzle as well as the effects of aerodynamic and geometric parameters on nozzle performance. Then an approximate model was established to characterize the complex system. With the *RSM* model, the effect of aerodynamic and geometric parameters was reappraised and the coupling effect between parameters was studied. Finally, a penalty function approach was used to optimize the parameter combination to reach the desired *RTAC* with limited secondary flow.

The flow characteristics of the hybrid *TC* nozzle lie in the fact that the subsonic flow is transversely injected into the high subsonic flow. The rotary valve and secondary flow disturbs the primary flow and control the effective flow area of the nozzle. When *NPR* is higher than 4, the change of *NPR* has little effect on *RTAC*, but C_{fg} increases with the increase of *NPR* from 4 to 14 because of the decrease of flow loss caused by overexpansion. The entrainment flow can make the flow loss reduce under the overexpansion condition. *RTAC* increases along with the increase of *SPR*, *θ*, *R* or A_s while C_{fg} changes inversely, and *η* is bigger than 5.24.

As for the hybrid *TC* nozzle, the effect of *NPR* and *SPR* is more significant than that of other parameters. The deflection angle of the rotary valve can be used to control *RTAC* effectively without worsening C_{fg} significantly. The coupling effect between multiple parameters can be revealed with the *RSM* model. What's more, the parameter combination can be optimized according to specified requirements and the maximal error of the optimization result compared with the CFD result is 4.13 percent. Another potential application of the approximate model is coupling the nozzle with the aero-engine and it will be done in further work.

REFERENCES

Baruzzini, D., N. D. Domel and D. N. Miller (2007) Pulsed injection flow control for throttling in supersonic nozzles – a computational fluidic dynamics design study. *37th AIAA Fluid Dynamics Conference and Exhibit*, FL, USA, AIAA-2007-4215.

Blaszak, J. J. and F. E. Fahrenholz (1960). Rocket thrust control by gas injection. *Massachusetts In- statute of Technology*, U.S.A, TR-430.

Catt, J. A., D. N. Miller and V. J. Giuliano (1995). A static investigation of fixed-geometry nozzle using fluidic injection for throat control. *31st Joint Propulsion Conference and Exhibit*, CA, USA, AIAA-95-2604.

Deere, K. A. (2003). Summary of fluidic thrust vectoring research conducted at NASA

Langley research center. *AIAA Applied Aerodynamics Conference*, Florida, USA. AIAA 2003-3800.

Domel, N. D., D. Baruzzini and D. N. Miller (2007). Pulsed injection flow control for throttling in supersonic nozzles – a computational fluidic dynamics based performance correlation. *37th AIAA Fluid Dynamics Conference and Exhibit*, FL, USA, AIAA-2007-4214.

Ferlauto, M. and R. Marsilio (2017). Numerical investigation of the dynamic characteristics of a dual throat nozzle for fluidic thrust vectoring. *AIAA Journal* 55(1), 86-98.

Heidari, M. R. and A. R. Pouramir (2016). Investigation and comparison effects of fluid injection type in thrust vector control. *Journal of Applied Fluid Mechanics* 9(1), 19-26.

Heo, J. Y. and H. G. Sung (2012). Fluidic thrust vector control of supersonic jet using coflow injection. *Journal of Propulsion and power* 28(4), 858-861.

Martin, A. I. (1957). The Aerodynamic variable nozzle. *Journal of Aeronautical Sciences* 24(5), 357-362.

Mason, M. S. and W. J. Crowther (2004). Fluidic thrust vectoring for low observable air vehicle, 2nd AIAA flow control conference, 28 June-1 Jule, 2004, Portiand Oregon. AIAA 2004-2210.

McArdle, J. G. (1958). Internal characteristics and performance of an aerodynamically controlled variable discharge convergent nozzle. *Lewis Flight Propulsion Laboratory*, Cleveland, U.S.A. NACA TN-4312.

Miller, D. N. and J. A. Catt (1995). Computational development of fixed-geometry nozzles for using fluidic injection for throat area control. *31st Joint Propulsion Conference and Exhibit*, CA, USA, AIAA-95-2603.

Miller, D. N., P. J. Yagle and E. E. Bender (2001). A computational investigation of pulsed injection into a confined, expanding crossflow. *31st AIAA Fluid Dynamic Conference & Exhibit*, California, USA, AIAA-2001-3026.

Shi, J. W., Z. X. Wang, L. Zhou and X. L. Sun (2020). Investigation on flow characteristics and performance estimation of a hybrid SVC nozzle. *Journal of Applied Fulid Mechanics* 13(1), 25-38.

Spaid, F. W. and E. E. Zukoshi (1968) A study of the interaction of gaseous jets from transverse slot with supersonic external flows. *AIAA Journal* 6(2), 205-212.

Thillaikumar, T., P. Bhale and M. Kaushik (2020). Experimental investigations on the strut controlled thrust vectoring of a supersonic nozzle. *Journal of Applied Fulid Mechanics* 13(4), 1223-1232.

Vakili, A. D., S. C. Sauerwein and D. N. Miller (1999). Pulsed injection applied to nozzle internal flow control. *37th AIAA Aerospace Sciences Meeting and Exhibit*, NV, USA. AIAA-99-1002.

Walker, S. H. (1997). Lessons learned in the development of a national cooperative program. *33rd Joint Propulsion Conference and Exhibit*, WA, USA. AIAA199-3348.

Younes, K. and J. P. Hickey (2020). Fluidic thrust shock-vectoring control: a sensitivity analysis. AIAA Journal 58(4), 1887-1890.

Zumwalk, G. W. and W. N. Jackomis (1962) Aerodynamic throat nozzle for thrust magnitude control of solid fuel rocket. *American Rocket Society Journal* 32(12), 1934-1936.